

Mg I emission lines at 12 & 18 μm in K giants[★]

J.O. Sundqvist¹, N. Ryde^{2,3}, G.M. Harper⁴, A. Kruger^{5, **}, and M.J. Richter^{5, **}

¹ Institut für Astronomie und Astrophysik der Universität München, Scheinerstr. 1, 81679 München, Germany
e-mail: jon@usm.uni-muenchen.de

² Department of Astronomy & Space Physics, Uppsala University, Box 515, 751 20 Uppsala, Sweden

³ Lund Observatory, Box 43, SE-221 00 Lund, Sweden

⁴ Center for Astrophysics and Space Astronomy, Astrophysics Research Lab, 593 UCB, University of Colorado, Boulder, CO 80309-0593, USA

⁵ Department of Physics, University of California at Davis, CA 95616, USA

Received 14/03/2008 / Accepted 22/05/2008

ABSTRACT

Context. The solar mid-infrared metallic emission lines have already been observed and analyzed well, and the formation scenario of the Mg I 12 μm lines has been known for more than a decade. Detections of *stellar* emission at 12 μm have, however, been limited to Mg I in very few objects. Previous modeling attempts have been made only for Procyon and two cool evolved stars, with unsatisfactory results for the latter. This prevents the lines' long predicted usage as probes of stellar magnetic fields.

Aims. We want to explain our observed Mg I emission lines at 12 μm in the K giants Pollux, Arcturus, and Aldebaran and at 18 μm in Pollux and Arcturus. We discuss our modeling of these lines and particularly how various aspects of the model atom affect the emergent line profiles.

Methods. High-resolution observational spectra were obtained using TEXES at Gemini North and the IRTF. To produce synthetic line spectra, we employed standard one-dimensional, plane-parallel, non-LTE modeling for trace elements in cool stellar atmospheres. We computed model atmospheres with the MARCS code, applied a comprehensive magnesium model atom, and used the radiative transfer code MULTI to solve for the magnesium occupation numbers in statistical equilibrium.

Results. The Mg I emission lines at 12 μm in the K giants are stronger than in the dwarfs observed so far. We present the first observed stellar emission lines from Mg I at 18 μm and from Al I, Si I, and presumably Ca I at 12 μm . We successfully reproduce the observed Mg I emission lines simultaneously in the giants and in the Sun, but show how the computed line profiles depend critically on atomic data input and how the inclusion of energy levels with $n \geq 10$ and collisions with neutral hydrogen are necessary to obtain reasonable fits.

Key words. Infrared: stars, Stars: atmospheres, Stars: individual (Pollux, Arcturus, Aldebaran), Stars: late-type, Line: formation

1. Introduction

Metallic solar emission lines around 12 μm were first identified by Chang & Noyes (1983), with the most prominent lines originating from transitions¹ $7i \rightarrow 6h$ (12.32 μm) and $7h \rightarrow 6g$ (12.22 μm) between Rydberg states of neutral magnesium. Additional Rydberg emission lines from Al I, Si I, and tentatively Ca I were identified as well (Chang & Noyes 1983; Chang 1984). The Mg I line formation scenario remained unclear until Chang et al. (1991) and Carlsson et al. (1992), hereafter C92, in two independent studies reproduced the emission

features by employing standard plane-parallel numerical radiative transfer with a detailed atomic model and a reliable solar atmosphere. They confirmed an origin below the atmospheric temperature minimum, refuted a chromospheric line contribution, and established a non-LTE (LTE: Local Thermodynamical Equilibrium) formation scenario. The solar lines have subsequently been used in, e.g., Mg I statistical equilibrium analysis by Zhao et al. (1998). C92 proposed a general Rydberg line formation mechanism for the highly excited metal lines, which implied that all visible metal emission lines in the solar spectrum around 12 μm originated in the photosphere. A detailed non-LTE modeling of the Al I emission has been carried out by Baumüller & Gehren (1996), where they confirmed this mechanism.

The lack of suitable spectrometers and the low stellar flux in the mid-infrared have in the past made high-resolution spectroscopy in this wavelength region possible only for the Sun and a few luminous nearby stars. Ryde et al. (2004) observed the 12 μm Mg I emission features in Procyon, and successfully reproduced the line profiles by employing the same modeling technique as C92. Uitenbroek & Noyes (1996) observed and modeled the evolved stars Arcturus (α Boo) and Betelgeuse (α Ori). Using the same model atom as C92, they were unable to fit the line profiles of the $7i \rightarrow 6h$ Mg I transition, which appeared both in emission (Arcturus) and absorption (Betelgeuse). Their observational

* Partly based on observations obtained at the Gemini Observatory, which is operated by the Association of Universities for Research in Astronomy, Inc., under a cooperative agreement with the NSF on behalf of the Gemini partnership: the National Science Foundation (United States), the Science and Technology Facilities Council (United Kingdom), the National Research Council (Canada), CONICYT (Chile), the Australian Research Council (Australia), CNPq (Brazil) and SECYT (Argentina).

** Visiting Astronomer at the Infrared Telescope Facility, which is operated by the University of Hawaii under Cooperative Agreement no. NCC 5-538 with the National Aeronautics and Space Administration, Science Mission Directorate, Planetary Astronomy Program.

¹ Quantum state nl , where n denotes the principal quantum number and l the orbital

sample also included five M giants and supergiants, in which the line appeared in absorption. However, Ryde et al. (2006) investigated water vapor lines for Betelgeuse in the same spectral region, and found a water line that coincided with the wavelength of the Mg I 12.32 μm line. The group successfully modeled the water line, without considering the Mg I blend (which we predict to be very weak, see Sect. 6.3). This may explain the sample of observed M star absorption at 12.32 μm , since water vapor is expected in these stars, whereas the Mg I emission line contribution should be minor.

A well known potential use for the Mg I lines is as probes of magnetic fields, which play a fundamental role in the underlying physics of a cool stellar atmosphere. Zeeman line-splitting from an external magnetic field increases quadratically with wavelength, while the Doppler broadening only has a linear dependence. Thus a line's sensitivity to magnetic fields becomes higher at longer wavelengths. The splitting of the solar emission lines was pointed out early and has been extensively analyzed. We have performed observations of the magnetically active dwarf ϵ Eridani. These will be reported on in a forthcoming paper (Richter et al., in preparation), hence we defer further discussions about stellar disk-averaged magnetic fields until then. Prior to (stellar) diagnostic applications, however, we should make sure that we are able to model and understand these lines in a range of stars. So far, as mentioned above, modeling attempts for evolved stars have been unsuccessful. We address this issue here by analyzing high-resolution observational spectra, which show strong Mg I emission lines in the three giants Pollux (K0 III), Arcturus (K1.5 III), and Aldebaran (K5 III). We model and analyze simultaneously the three K giants and the Sun, with particular emphasis on influences from atomic data, and discuss why previous modeling attempts have not succeeded. The organization of the paper is as follows; in Sect. 2, we describe the observations. In Sect. 3 we review some concepts about the formation of the infrared Mg I emission lines and in Sect. 4 we describe our modeling procedure. Results are presented in Sect. 5 and we discuss them and give our conclusions in Sect. 6.

2. Observations

The observations were made with TEXES, the Texas Echelon-cross-echelle Spectrograph, Lacy et al. (2002). TEXES provides high spectral resolution in the mid-infrared and is available as a visiting instrument at both Gemini North and at IRTF, the Infrared Telescope Facility. The Pollux (β Gem) observations come from the November 2006 observing campaign at Gemini North. The Arcturus and Aldebaran (α Tau) observations were done over many years at the IRTF. In most cases, the observations were primarily intended for flux calibration or focus tests and not to study the stars themselves.

When observing stars with TEXES, we nod the source along the slit, typically every 10 seconds, to remove sky and telescope background. Before each set of 8 to 16 nod pairs, we observe a calibration sequence that includes an ambient temperature blackbody and an observation of blank sky emission. The difference of blackbody minus sky serves as a first order telluric correction and flatfield. Where possible, a featureless continuum object with emission stronger than the target is also observed to further correct for telluric features and flatfielding. The largest asteroids work very well for this purpose, as does Sirius (α CMa) with respect to Pollux.

At the frequencies of the mid-infrared Mg I emission lines, the spectral orders from the TEXES high-resolution echelon grating are larger than the 256^2 pixel detector array. This results in

slight gaps in the spectral coverage. For the Pollux observations, which were the final observations before sunrise, we observed in two settings and adjusted the tilt of the collimator mirror feeding the echelon grating for the second setting. This shifts the spectral orders in the dispersion direction. By combining the data from these separate observational settings, we were able to fill in the gaps in the spectral orders. The Arcturus and Aldebaran data were constructed from many separate observing settings and no particular efforts were made to fill in the gaps.

Data reduction was done using a custom FORTRAN pipeline (Lacy et al. 2002). The pipeline corrects for spikes and optical distortions in the instrument, allows the user to set the wavelength scale based on telluric atmospheric features, flatfields the data, differences nod pairs to remove the background emission, and then combines the resulting differences. Finally it extracts a spectrum based on the spatial information within the two-dimensional echellogram. The pipeline also provides a fairly accurate estimate of the relative noise in each pixel.

To combine data from separate observations, we first established a common wavelength scale. We corrected each spectrum for the Earth's motion at the time of the observation and then interpolated the data onto the common scale. We used a fourth-order polynomial derived from line free regions to normalize each spectral order. We determined the signal-to-noise (S/N) for the normalized spectrum via a Gaussian fit to pixel values and used the relative noise estimate established during pipeline reduction to assign a weight for each spectral pixel. When combining data, we choose to weight by the signal-to-noise squared, which effectively means weighting by successful observing time.

Observations of low pressure gas cells near 13.7 μm at the November 2006 run indicate that the instrumental profile for the 12 μm observations of Pollux has a Gaussian core with a FWHM $\sim 3.0 \text{ km s}^{-1}$, corresponding to a spectral resolution $R \sim 10^5$. As the Arcturus and Aldebaran spectra combined data from four different runs and possible errors from the combinations may be significant, we were unable to make a reliable measurement of the instrumental profile in this region for these stars. At 18 μm , similar measurements indicate that these observations have a Gaussian instrumental profile with a FWHM $\sim 4.5 \text{ km s}^{-1}$. In Sect. 5 we display our observed data re-binned to approximately the spectral resolution, except for Fig. 5, where the pixel scale is used. Signal-to-noise ratios in the spectra vary but are generally high, reaching $S/N \sim 450$ per pixel for Pollux and ~ 300 for Arcturus and Aldebaran, in regions around the 12.22 μm line. At 18.83 μm , the ratio is $S/N \sim 40$.

3. Departure coefficient ratios

Before proceeding to a modeling description, we briefly review some important concepts about the formation of the 12 μm emission lines. In the following we use the departure coefficients $b_i = n_i/n_i^*$, where n_i is the actual number density (not to be confused with the principal quantum number n) of energy level i and n_i^* the corresponding LTE population, as calculated from the total magnesium abundance using the complete Saha-Boltzmann relations. In a spectral line, a departure coefficient ratio which differs from unity, $b_l/b_u \neq 1$, at line-forming depths causes a deviation of the line source function, S_ν^l , from the Planck function, B_ν , which affects the emergent intensity:

$$\frac{S_\nu^l}{B_\nu} = \frac{e^{h\nu/kT} - 1}{b_l/b_u \times e^{h\nu/kT} - 1} \quad (1)$$

For a characteristic wavelength $\lambda = 12.3 \mu\text{m}$, and temperature $T = 5000 \text{ K}$, we get $e^{h\nu/kT} \sim 1.26$, and may directly from Eq. 1

realize that already a small deviation from unity in the departure coefficient ratio causes a significant change in the line source function. The physical reason for this is the increasing importance of stimulated emission in the infrared. If $b_u/b_l > 1$ and increases outwards in the atmosphere, we may get a rising total source function and a line profile appearing in emission despite an outwards decreasing temperature structure. Such departure coefficient divergence occurs between highly excited Rydberg levels in the outer layers of the modeled stellar photospheres considered in this study, and is the reason for the modeled emission lines.

Departure coefficient ratios that deviate from unity are set up by three-body recombination from the Mg II ground state and a ‘de-excitation ladder’ that preferably takes $\Delta n, \Delta l = -1$ downward steps (see Fig. 1 for an illustration). In the solar case, all Mg I Rydberg levels are strongly collisionally coupled to each other and to the Mg II ground state. The main effects that drive the line source function out of LTE come from lines elsewhere in the term diagram, primarily lines between levels with intermediate excitation energies, which are optically thin in the outer atmosphere and experience photon losses (Rutten & Carlsson 1994). These levels impose a lower limit to the Rydberg state deexcitation ladder. The number densities of the Rydberg energy levels adjust to the upper and lower limits, and a radiative-collisional population flow occurs. It was shown, for the solar case by C92, how a high probability for $\Delta n, \Delta l = -1$ downward transitions is necessary for the Rydberg state ladder to be efficient and that these transitions dominate only if the collisional coupling is strong in the uppermost Mg I levels. It was also shown how this high probability arises from the regular character of the collisional cross-sections of transitions between highly excited levels. We thus remind of the remark in C92 that for a correct description of the ladder flow between highly excited levels, it is more important to have a *consistent* set of collisional data, than to have the most accurate cross-sections for a few transitions. These considerations are important to keep in mind when we later discuss our extension of the model atom and the influence from collisions with neutral hydrogen. A more comprehensive description of non-LTE effects throughout the Mg I term diagram that affect the solar 12 μm lines can be found in Rutten & Carlsson (1994).

4. Modeling

To produce synthetic line spectra, we employ standard one-dimensional, plane-parallel, non-LTE modeling for trace elements in cool stellar atmospheres. We generate model atmospheres from the MARCS code (Gustafsson et al. 1975, 2008), adopt a comprehensive magnesium model atom, and use the radiative transfer code MULTI (Carlsson 1986, 1992) to solve for the magnesium occupation numbers in statistical equilibrium, while holding the structure of the atmosphere fixed.

4.1. Model atmospheres and stellar parameters

The MARCS hydrostatic, plane-parallel models are computed on the assumptions of LTE, chemical equilibrium, homogeneity, and the conservation of the total flux (radiative plus convective; the latter treated using the mixing-length theory). No chromospheric temperature rise is invoked but, as shown by C92, omitting a chromosphere has a negligible impact on the solar Mg I 12 μm transitions. The findings in this work and that by Ryde et al. (2004) suggest that this holds true also for other investigated stars. Apart from the temperature and density stratifi-

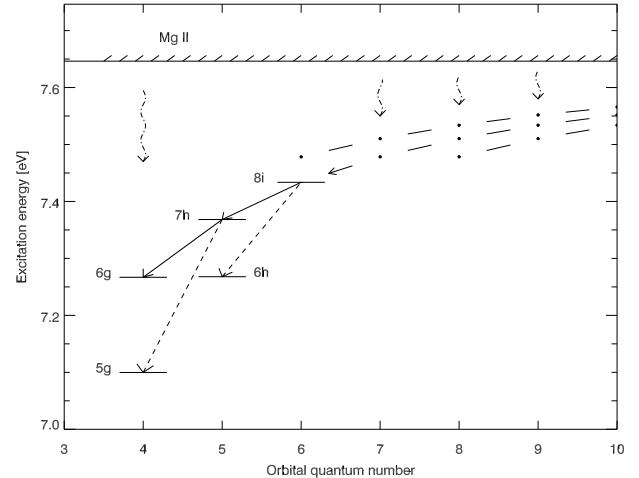


Fig. 1. Illustration of the ‘Rydberg ladder’ (see text), using a *selected* part of the Mg I term diagram. Five levels about the $7h \rightarrow 6g$ transition are labeled with corresponding quantum numbers nl . Dots mark energy levels with $n \geq 9$ and $l \geq n - 3$. Solid lines between levels show transitions with $\Delta n, \Delta l = -1$, dashed show two alternative transitions ($\Delta n = 2, \Delta l = -1$). Dashed-dotted illustrate recombination from the Mg II continuum.

cations, a detailed MARCS radiation field was generated using opacity samplings including millions of lines. A sampled version of this radiation field was used when MULTI calculated the photoionization rates, in order to properly account for the line-blocking effect. We discuss some variations to our procedure in Sect. 6.

The stellar parameters we used for Pollux were $T_{\text{eff}} = 4865$ K, $\log g = 2.75$ (cgs), a solar metallicity (as given by Grevesse et al. 2007), and a depth independent ‘microturbulence’ $\xi = 1.5$ km s $^{-1}$, all based on a spectral analysis of optical iron and calcium lines made by Drake & Smith (1991). For the parameters of Aldebaran we adopted $T_{\text{eff}} = 3900$ K, $\log g = 1.5$ (cgs), a metallicity² $[M/H] = -0.25$, and $\xi = 1.7$ km s $^{-1}$. These are from primarily Decin et al. (2003) but considering also sources accessible at the SIMBAD astronomical database. Finally for Arcturus we used $T_{\text{eff}} = 4280$ K, $\log g = 1.5$ (cgs), $[M/H] = -0.50$, and $\xi = 1.7$ km s $^{-1}$. A discussion of these Arcturus parameters can be found in Ryde et al. (2002). The stars are all nearby and well-studied objects, and their parameters should be fairly accurate. Model grids show that the effects on the lines from (reasonable) variations in $\log g$ or T_{eff} are smaller than effects from, e.g., atomic input data, which will be investigated in the following sections.

We convolved our computed intrinsic line profiles with the instrumental profile, the projected rotational velocity ($v \sin i$), and the ‘macroturbulence’ (none of which affect the line strength but only the profile shape). We adopted $v \sin i$ values from Smith & Dominy (1979), which for Pollux, Arcturus and Aldebaran are, respectively, $v \sin i = 0.8, 2.7, 2.7$ km s $^{-1}$. As we were unable to obtain a fair estimate of the instrumental profile for the Arcturus and Aldebaran spectra around 12 μm , we choose first to assign an isotropic Gaussian shape with charac-

² Here we do not specify individual metal abundances, but $[M/H]$ is taken as the characteristic metallicity where as usual $[A/B] = \log(n_A/n_B)_* - \log(n_A/n_B)_\odot$.

teristic Doppler velocity v_m for the combined effect of the instrumental profile and the macroturbulence. For Pollux, where the instrumental profile could be separated out, we obtained $v_{macro} \sim 3.3 \text{ km s}^{-1}$. However, it became clear that the modeled line wings of the K giants better fitted the observations when assuming a radial-tangential Gaussian shape (Gray 1976) for the macroturbulence. Therefore we decided to assign the Pollux instrumental profile for all three stars (the exact values are not so significant since the macroturbulence is the dominating external line broadening), and adopted a radial-tangential macroturbulence $v_{m,R-T} = 5.5, 6.0, 5.5 \text{ km s}^{-1}$ to fit the observed line-widths. Our values are $\sim 2 \text{ km s}^{-1}$ higher than those measured from Fourier analysis in optical spectra by Smith & Dominy (1979).

4.2. The model atom

Our Mg I model atom is essentially an enlarged and slightly modified version of the one compiled by C92, and a full description can be found there. The original model atom has also been used in the analysis of solar magnetic fields (e.g., Bruls et al. 1995), for the Mg I 12 μm flux profiles of Procyon (Ryde et al. 2004), and in a previous attempt to model giants (Uitenbroek & Noyes 1996). In short, the atom is complete with all allowed transitions up to principal quantum number $n = 9$ and includes the ground state of Mg II. We now describe changes and tests we have made.

4.2.1. Enlargement of the model atom

Lemke & Holweger (1987), who also pointed out a possible photospheric line-origin through a rising line source function, made a statistical equilibrium investigation for the Sun but were unable to reproduce the Mg I 12 μm emission due to a combination of their adopted collisional data treatment and an inadequate model atom. Their exclusion of levels higher than $n = 7$ resulted in an incorrect description of the replenishment of the Rydberg levels from the ion state. C92 experimented with the $n = 8, 9$ levels and confirmed that these were necessary to have top-levels that were fully dominated by collisions and to obtain sufficient departure coefficient differences in line-forming layers to match the observed solar emission features. In this work we have extended the model atom to include levels with $n \geq 10$ to investigate if the departure coefficient differences are further enhanced.

The model atom was first enlarged to include all energy levels and allowed transitions with $n = 10$. To ensure homogeneity throughout the model atom, all new atomic data were calculated using the same formalisms as those employed by C92. The only exception was absorption oscillator strengths for transitions with $l \leq 3$ for which data was drawn from the opacity project (OP) TOP-BASE (Cunto & Mendoza 1992), since the tabulation used by C92 (Moccia & Spizzo 1988) only extend to $n = 9$. The enlargement caused an upward shift in the Mg I departure coefficients, and the effect became more pronounced as n increased; thus producing larger departure coefficient differences between adjacent levels. The same effect was seen in the Mg I statistical equilibrium for all our template atmospheres. To investigate the influence of the low l levels, a test-run was also made where only $n = 10$ levels and transitions with $l \geq 4$ were included. This model atom and the complete $n = 10$ atom produced almost indistinguishable results.

After this initial enlargement, atomic models were constructed step-wise, including higher principal quantum numbers. The en-

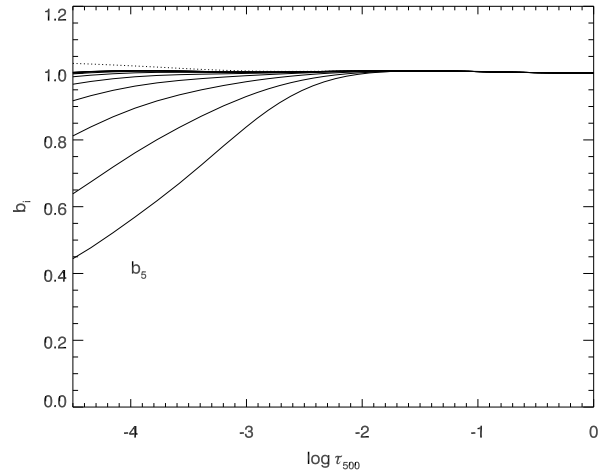


Fig. 2. Solar departure coefficients for Rydberg state energy levels with $n \geq 5$, as functions of the continuum optical depth at 500 nm. b_5 is indicated in the figure, and an increment of one follows upwards in the figure. The displayed coefficients combine all $b_{n,l}$ coefficients with the same n and $l \geq 4$. The Mg II ground state is labeled with dots.

hancement continued until the atom's uppermost n level and the second uppermost were Boltzmann populated with respect to each other at all atmospheric layers (i.e., $b_{top-1}/b_{top} = 1$). This criterion was met for all atmospheric models when reaching $n = 15$, illustrated for the solar case in Fig. 2 (where our model actually meets the criterion already at $n = 12$). Sensitivity tests verified that no differences in results occurred when adding the final $n = 15$ top-levels. The main difference between the solar departure coefficients (Fig. 2) and those of the K giants is that the latter have Mg II ground states that are more overpopulated relative to LTE in their outer atmospheres. This is mainly because Mg I and Mg II are competing ionization states in these cooler atmospheres, so that the ion ground state becomes more sensitive to deviations from LTE in Mg I population densities. In Arcturus and Aldebaran, the overionization is further enhanced by the lower metallicity, which reduces the important line-blocking effect.

As the influence from levels with low l was negligible already for $n = 10$, we have confined the enlargement to levels and transitions with $l \geq 4$.

4.2.2. Collisional data

Ryde et al. (2004) compared *radiative* bound-bound and bound-free data from our model atom with OP data and found an overall good agreement. We have therefore restricted our analysis here to some aspects of the *collisional* data, which usually introduce the largest uncertainty in the model atom, due to a large number of poorly known cross-sections.

4.2.3. Collisions with neutral hydrogen

The role of collisions with neutral hydrogen in cool stellar atmospheres has long been a subject for debate. Despite small cross-sections (as compared to electron impacts), one may expect them to contribute significantly to collisional rates due to large n_{HI}/n_e ratios. In the outer parts of the model atmospheres in this study,

this ratio ranges from about 10^4 in the Sun to 10^5 in the cooler and more metal-poor Arcturus. No collisions with neutral hydrogen were considered in the original model atom.

When inelastic collisions with neutral hydrogen are explicitly included in non-LTE calculations, a standard procedure is to adopt the recipe of Drawin (1969), as given by Steenbock & Holweger (1984). The Drawin formula has often been criticized. Steenbock & Holweger state an accuracy of an order of magnitude, but a rather common remark is that the recipe may overestimate the cross-sections with as much as one to six orders of magnitudes (see, e.g., Asplund 2005, and references therein). Unfortunately, more reliable cross-sections are scarce, especially for non-LTE calculations that require data for a large set of transitions. A customary way around this shortage is to adopt a scaling factor S_{H} to the Drawin formula, calibrated on solar or stellar observations.

In studies concerning the solar Mg I 12 μm lines, the Drawin formula was adopted by Lemke & Holweger (1987) and Zhao et al. (1998). The latter group scale their values with a factor that decreases exponentially with increasing excitation energy. Consequently, they apply $S_{\text{H}} = 3 \times 10^{-10}$ for the 12 μm transitions, which give them essentially the same result as if neglecting hydrogen collisions. Recall also that the former group was unsuccessful in producing an emission line core in their statistical equilibrium analysis.

Here we have estimated the collisional rates due to neutral hydrogen impacts using the Drawin formula. When introduced without scaling factor, our models reveal solar 12 μm lines in pure absorption and this case will therefore not be considered. By calibrating on the solar observations, we have adopted $S_{\text{H}} = 10^{-3}$ in all computations involving collisions with neutral hydrogen. However, in view of the existing uncertainties, we present results both from including these collisions for all radiatively allowed bound-bound (for which we have oscillator strengths) and all bound-free transitions, and excluding them.

4.2.4. Collisional excitation from electrons

The bulk of the collisional cross-sections from electron impacts for radiatively allowed transitions are calculated, as was done in C92, using the impact parameter approximation (Seaton 1962). Mashonkina (1996) showed that, overall, this approach predicts significantly smaller cross-sections than the alternative semi-empirical formula of van Regemorter (1962) (applied for the solar Mg I lines in, e.g., Zhao et al. 1998). Avrett et al. (1994) used both formalisms when modeling the solar Mg I lines and concluded that using van Regemorter gave somewhat weaker emission. In C92, the impact parameter approximation is claimed to give a consistent set of rates accurate to within a factor of two for transitions between closely spaced levels.

Note that the above mentioned formalisms relate the collisional cross-section to the oscillator strength and may therefore not be applied to radiatively forbidden transitions. The ‘forbidden’ cross-sections are here set to a multiplying factor times that of the closest allowed (see C92). The original choice (C92) for this factor was 0.05, but Bruls et al. (1995) discovered some errors regarding a few oscillator strengths, accounted for here as well, and the factor was revised to 0.3 in order to reproduce the previous results. We also adopt 0.3, which was used by Ryde et al. (2004) as well. A similar treatment for solar Mg I analysis has been used by Mauas et al. (1988) who assumed 0.1, the same value as estimated in Allen (1973). Sigut & Lester (1996) also adopted 0.1 for Mg II (in work where they, for B type stellar photospheres, predicted the corresponding Rydberg emission lines

for Mg II), which they found to be in rough agreement with a few more rigorously calculated rates from low excitation transitions. We have tested using the enlarged model atom without collisions with neutral hydrogen and concluded that by a raise to 0.7 times the cross-section of the nearest allowed transition we are able to reproduce the observed solar lines, but that the modeled emission in the K giants remain far lower than the observed. An alternative approach for the radiatively forbidden transitions, applied in, e.g., Mg I (and II) non-LTE abundance analyses (Zhao et al. 1998; Przybilla et al. 2001; Gehren et al. 2004; Mashonkina et al. 2008), is to set a constant collisional strength $\Omega = 1$. Overall, this gives considerably lower collisional rates. The collisional strength Ω for collisions with electrons is related to the Maxwellian averaged downward collisional rate C_{ji} [s^{-1}] via:

$$C_{ji} = 8.63 \times 10^{-6} \Omega T_e^{-1/2} g_j^{-1} n_e \quad (2)$$

where T_e is the electron temperature, g_j the statistical weight of the upper level, and n_e the number density of free electrons. The upward rate, C_{ij} , then follows from the principle of detailed balance. We have also tested assuming a constant $\Omega = 1$ on the solar and Arcturus model, and verified that the modeled emission for Arcturus still is inadequate, remaining on the same low level as that displayed in Fig. 3, when collisions with neutral hydrogen are not included. The solar emission increases by this approach, but not enough to drastically change the suitable S_{H} factor. Overall, our experiments with the radiatively forbidden transitions tell us that the solar emission lines are somewhat sensitive to these rates, whereas the models of the K giants are much less responsive.

4.2.5. l-changing collisions

No explicit calculations of collisional transitions of type $n, l \rightarrow n, l'$ with high orbital quantum numbers ($l' \geq 4$) were made in the original model atom, but rather it was assumed that these collisional rates were high enough to ensure strong coupling between closely spaced levels. This was established by setting $\Omega = 10^5$ if the difference in effective principal quantum number ($n - \delta$ where δ is the quantum defect) in the transition was less than 0.1. The high value of Ω causes very high collisional rates, which essentially force all levels with the same n and $l \geq 4$ to share a common departure coefficient (i.e., to be Boltzmann populated with respect to each other), in agreement with the proposed assumption. This, however, only holds for all relevant atmospheric layers in the Sun, whereas in the more diluted model atmospheres of the K giants, we find deviations between departure coefficients in outer layers (for Arcturus outside $\log \tau_{500} \sim -2$) for levels with relatively low orbital quantum numbers, when setting $\Omega = 10^5$. Apparently, such a value does not suffice for the K giants and we need to either raise the factor or explicitly estimate the rates. Note that C92 based the assumption of common departure coefficients mostly on the large cross-sections for l -changing collisions with neutral hydrogen calculated by Omont (1977), cross-sections later shown to be over-estimated by an order of magnitude (Hoang-Binh & van Regemorter 1995).

In this work, we have calculated explicit electron/ion collisional rates for transitions with $\Delta l = \pm 1, \Delta n = 0$ and $l, l' \geq 3$ by using a cut-off at large impact parameters, as outlined by Pengelly & Seaton (1964). We find that the radial cut-off for transitions with low l is set by the non-degeneracy of the energy levels. For ion rates, this happens inside the radius where the strong interaction dominates and hence the impact parameter approximation is not expected to be reliable. However, for

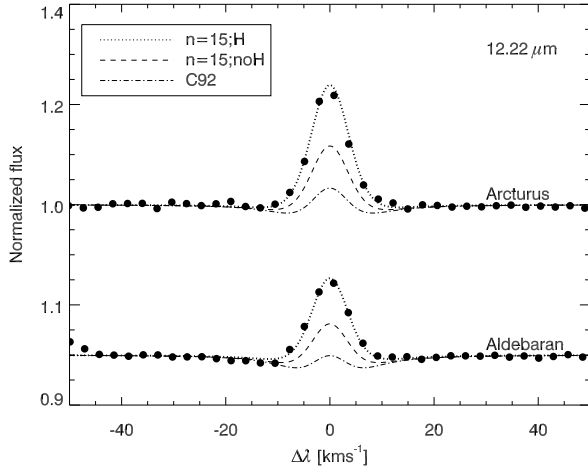


Fig. 3. Observed and modeled line profiles in Arcturus and Aldebaran for the 12.22 μm line, plotted on a velocity scale. Labels as indicated in the figure; where C92 denotes the original model atom, $n=15;\text{noH}$ the extended excluding collisions with neutral hydrogen and $n=15;\text{H}$ the one including such. The filled dots denote the observed data.

electron impacts the cut-off is at larger distances and since electron rates dominate over ion rates for these transitions, our approach should provide rates accurate to at least an order of magnitude also in the low l range. Ion rates surpass electron rates from $l \sim 9$ and higher, where the cut-off is well within the weak-interaction limit. We assume only singly ionized elements ($n_{\text{ion}} = n_e$) with the largest electron/ion donor being magnesium, providing $\sim 40\%$ of the total electron/ion pool in the relevant atmospheric layers in our MARCS models.

The calculated rates are in good agreement with the electron rates tabulated in Hoang-Binh & van Regemorter (1994), who exclusively considered l -changing collisions for the $n = 6, 7$ levels. Our rates are higher than those inferred from $\Omega = 10^5$ (by typically a factor of ~ 4 for, e.g., $n = 7$), hence no changes in results occur for the solar atmosphere. For the K giants, small differences between departure coefficients with the same n and $l \geq 4$ still exist but effects from using explicit rates are small. When forcing common departure coefficients for all equal n levels with $l \geq 4$ (by drastically increasing our computed rates), we still obtain normalized emission peaks for the K giants that differ only by a few percentage points.

5. Results

5.1. Emission lines at 12 μm

We plot observed and computed line profiles for the Mg I 12 μm lines in the Sun, Pollux, Arcturus, and Aldebaran in Figs. 3, 4 and 5. In Arcturus and Aldebaran, the 12.32 μm line is blended with a water vapor absorption line (see Ryde et al. (2006) for an identification), which in the latter star is so influential that we choose to exclude the Aldebaran 12.32 μm line from the analysis. The observed emission lines from the K giants are stronger than the solar lines. In addition to the Mg I lines, we also identify emission lines from Si I, Al I, and Ca I in the observed spectra of Pollux and Arcturus (three of the lines are displayed in Fig. 5), all identified as $n = 7 \rightarrow 6$ transitions with high orbital quantum numbers. The flux maximum in the observed and normalized

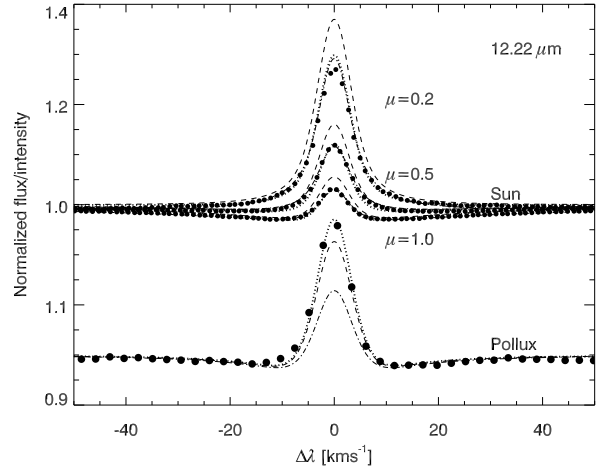


Fig. 4. Observed and modeled line profiles in Pollux and for three positions on the solar disk (indicated in the figure) for the 12.22 μm line, plotted on a velocity scale. Labels as in Fig. 3.

spectra (and the FWHM for the Mg I lines) are given in Tables 1 and 2. More line data can be found in Chang & Noyes (1983) and Chang (1984). We have also added results from modeled Mg I flux profiles for the Sun (from a disk integration over solar intensity profiles in a model that reproduces the observations) in Table 1, to enable a fair comparison between solar and stellar observations. This illustrates that the K giants have stronger emission than the Sun.

The line-center average depth of formation in the modeled Mg I 12 μm lines is, for the Sun and Pollux, in atmospheric layers slightly below $\log \tau_{500} \sim -3$, with the weaker 12.22 μm line shifted approximately 0.2 dex toward the inner photosphere. In Arcturus and Aldebaran, the line formation takes place deeper inside the atmosphere. The average depth of formation for the line-center in the 12.22 μm line in Arcturus and Aldebaran is $\log \tau_{500} = -1.8$ and -1.6 respectively. This is partly because of the lower amount of H_{ff}^- opacity in these atmospheres (due mainly to lower electron abundances), which shifts the continuum formation to about $\log \tau_{500} \sim -0.8$, as compared with $\log \tau_{500} \sim -1.2$ in Pollux.

The extension of the model atom has a significant impact on the synthetic line spectra, with computed intensity/flux profiles being much stronger when using the enlarged model atom. We note the failure of the smaller atom to reproduce the observed emission for the K giants, whereas it provides a good match for the solar lines, in agreement with previous studies. The larger model atom without collisions with neutral hydrogen predicts emission lines well below the observed level for Arcturus and Aldebaran, in contrast to the Sun where the modeled lines now are too strong. However, when including collisions with neutral hydrogen (as described in Sect. 4.2.3) the models reproduce the observed emission in all cases. These different responses to the ‘added’ collisions demonstrate the complexity of the Rydberg state deexcitation ladder, and are further discussed in Sect. 6.2.

Our models predict narrow absorption troughs in the Pollux lines, only matched by observations in the red wing of the 12.22 μm line. However, due to uncertainties in the observed normalized spectra imposed by, e.g., the continuum setting, we are not able to draw any firm conclusions from the absence of absorption troughs. A discussion about shifts in the solar absorption troughs, visible in Fig. 5, can be found in, e.g., Chang (1994).

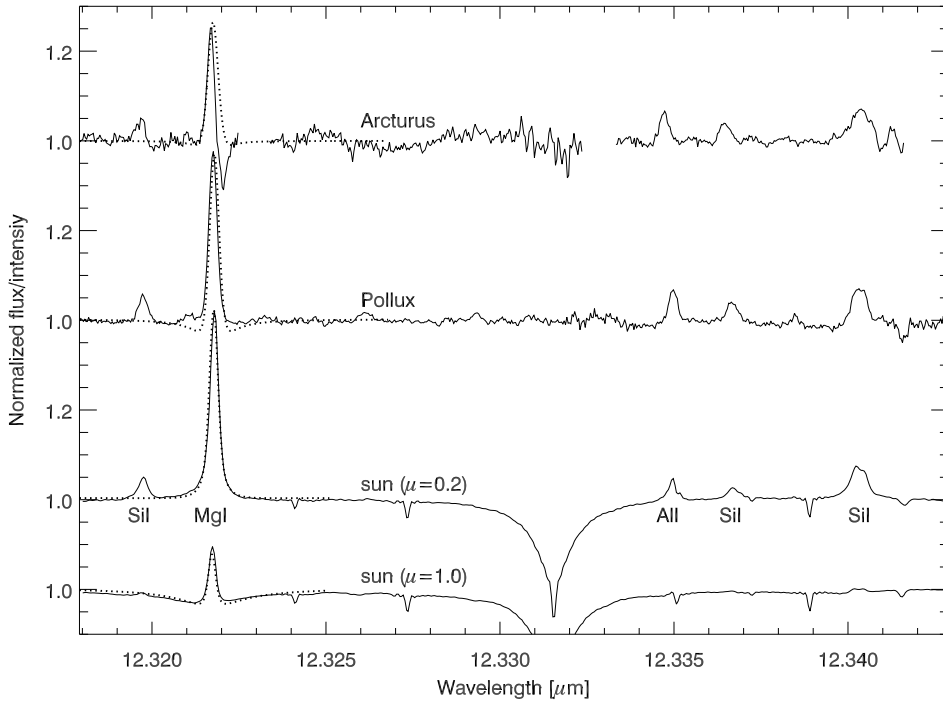


Fig. 5. Observed spectra around the 12.3 μm region, shifted to the solar frame, for Pollux, Arcturus, and for two positions on the solar disk (indicated in the figure). Solar observations are from Brault & Noyes (1983). Models for the Mg I 12.32 μm line are labeled with dots, and use the $n=15;H$ model atom (see Fig. 3). The solar absorption features are telluric lines, and the missing parts in the Arcturus spectrum are due to gaps between spectral orders. Visible emission lines as indicated in the figure. The Arcturus absorption line at 12.32 μm is a water vapor line.

We also note how the line-wings in Arcturus and Aldebaran are too broad to be fitted by an isotropic Gaussian, and require a radial-tangential macroturbulence (see Sect. 4.1).

5.2. Mg I emission lines at 18 μm

We also observed the $8h \rightarrow 7g$ Mg I transition at 18.83 μm in Pollux and Arcturus, and present here the first stellar observations of this line. The emission is high here as well, see Fig. 6 and Table 1. Our synthetic line spectra reproduce the observed emission also for this line, which suggest that our model atom accounts for the Rydberg state deexcitation ladder in an accurate way. For comparison reasons, we display also a solar disk-center intensity profile³. The observed solar line feature is barely visible, which further illustrates the stronger emission from K giants.

The difference between departure coefficients in $n = 8 \rightarrow 7$ transitions is of similar magnitude as that between 7 and 6, causing comparable emission line strengths. The continuum formation is shifted about 0.3 dex outwards when compared to the spectral region around 12 μm (the H_{I}^- opacity increases) but the average height of formation for the line-center in the 18.83 μm line in Pollux is located at $\log \tau_{500} \sim -2.5$, slightly further in than the 12 μm lines. This is because the line is merely the third strongest $8l \rightarrow 7l'$ transition with $\Delta l = -1$. We thus predict that the next two Rydberg transitions in the chain ($8i \rightarrow 7h$ located at 18.99 μm and $8k \rightarrow 7i$ at 19.03 μm) should appear even stronger, however these were not covered in our observational setup.

6. Discussion and conclusions

The model atom extension and the introduction of collisions with neutral hydrogen remove the discrepancy between observed and modeled emission in our study. *Before* the model atom was

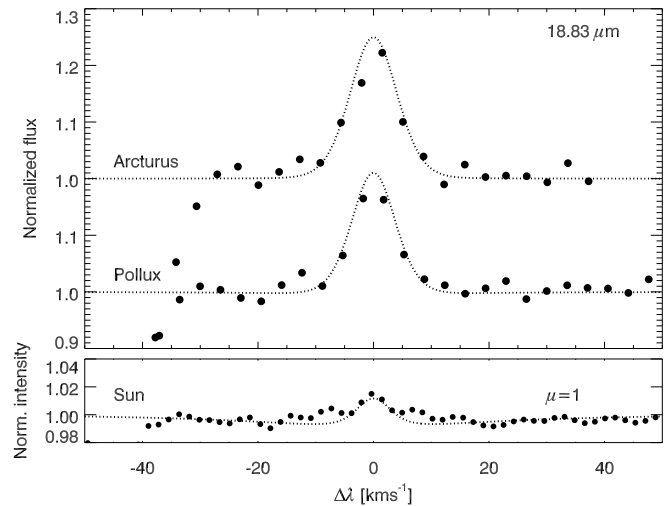


Fig. 6. Observed and modeled line profiles for the 18.83 μm line in Pollux, Arcturus, and at the solar disk-center. Labels as in Fig. 3. The feature to the left in the figure is an OH absorption line. Note the scale difference between the upper and lower ordinate.

Table 1. Summary of observed magnesium emission line properties.

Star, line [μm]	Normalized flux maximum			FWHM [km s^{-1}]		
	12.22	12.32	18.83	12.22	12.32	18.83
Pollux	1.28	1.37	1.20	6.8	7.1	8.2
Arcturus	1.24	^a	1.23	8.0	^a	9.7
Aldebaran	1.16	^a	-	8.0	^a	-
Sun ^b	1.09	1.15	-	5.8	6.1	-

^a Emission line blended with H_2O absorption line.

^b Modeled solar flux profiles (see text).

³ Observations from the Kitt Peak solar atlas

Table 2. Summary of observed emission line properties around 12 μm (other elements than magnesium) for Pollux and Arcturus.

Element ^a	Wavenumber ^b		Normalized flux maximum	
	Wavelength		Pollux	Arcturus
	[cm^{-1}]	[μm]		
Si I	810.360	12.340	1.07	1.08
Si I	810.591	12.337	1.04	1.04
Al I	810.704	12.335	1.07	1.06
Si I	811.709	12.320	1.06	1.05
Si I	813.380	12.294	1.06	1.07
Si I ^c	814.273	12.281	1.04	-
Ca I ^d	814.969	12.270	1.05	1.02
Al I ^c	815.375	12.264	1.03	-
Si I ^c	815.979	12.255	1.03	-

^a Line identifications based on Chang & Noyes (1983) and Chang (1984).

^b From the solar observations by Brault & Noyes (1983).

^c Emission line blended with OH absorption line.

^d Line identification in Chang & Noyes (1983) stated as ‘suspicious’.

extended, we undertook a number of tests to investigate the large discrepancies between observations and models. We therefore start our discussion by a short summary of these, with the purpose to simplify future work.

The lines are sensitive to the photoionization rates as these affect the recombination to the Rydberg levels. We thus made an *ad-hoc* increase in the photospheric MARCS radiation field until the modeled Mg I emission lines matched the observed, but found that the required additional mean intensities gave rise to surface fluxes that by far exceeded observed ones. We included a chromospheric temperature-rise in Arcturus and found it to have a negligible impact, with the lines forming in atmospheric layers below the temperature minimum. We computed MARCS models in spherical geometry and employed the spherical version of MULTI, S-MULTI (Harper 1994), but differences from plane-parallel models were small. No attempt to analyze influences from atmospheric inhomogeneities has been made in this work. A discussion about how granulation affects the solar lines can be found in Rutten & Carlsson (1994).

6.1. The model atom extension

All Mg I departure coefficients are shifted upwards (increased) by the extension of the model atom, but the upward shift is more pronounced in the higher energy levels. It is this change in the departure coefficient *ratio* in the line-forming regions that is sufficient to cause a significant change in results, i.e., higher emission peaks for the larger atom. The enhanced collisional coupling in the uppermost Mg I levels and to the Mg II ground state strengthens the cascading process in rather the same manner as the model atom with top-levels $n = 9$ did when compared to one reaching only $n = 7$ (see Sect. 4.2.1). Qualitatively, more recombinations enter at the top-levels, channel down through transitions that take part of the Rydberg ladder (see Fig. 1) and set up larger departure coefficient differences between adjacent levels. The extension thus has a significant impact on the mid-infrared emission lines, whereas the overall character of the Mg I statistical equilibrium remains.

To include the energy levels with $n \geq 10$ seems especially pertinent when applying the model atom on diluted stellar atmo-

spheres with low surface gravities (as shown by the large differences in the modeled line profiles of the K giants). These are more influenced by radiative transitions, and thus the extension ensures that the Rydberg level replenishment from the ion state is properly accounted for by including top-levels that are fully dominated by collisions.

6.2. Effects from extra collisions

Higher rates of collisional excitation and ionization affect the 12 μm lines in the implemented stellar model atmospheres differently. Figs. 3 and 4 show how (by the introduction of collisions with neutral hydrogen) the Mg I 12 μm emission is reduced in the Sun, increased in Arcturus and Aldebaran and almost unchanged in Pollux. Apparently, a homogeneous increase of collisional rates actually results in stronger emission in the low surface gravity atmospheres of Arcturus and Aldebaran (which one would perhaps not expect since, generally, collisions act to thermalize lines toward LTE).

We have analyzed this result by computing additional models for the Sun and Arcturus, where we included radiatively allowed bound-bound collisions with neutral hydrogen for 1) only the three transitions $7i \rightarrow 6h$, $7h \rightarrow 6g$, and $7g \rightarrow 6f$ and 2) only transitions with $\Delta n, \Delta l = -1$ and $n \geq 8$ and $l \geq 4$. The first test imposes stronger collisional coupling only in the $n = 7 \rightarrow 6$ transitions themselves, whereas the second serves to strengthen the collisional bound-bound coupling in transitions in the uppermost levels that take part of the Rydberg ladder (see Fig. 1), while maintaining all other rates.

We quantify the results of this experiment by the normalized flux maximum in the 12.22 μm line. In the first case, both models give lower emission, as expected from the direct thermalizing effect on the $n = 7 \rightarrow 6$ transitions. The modeled flux maximum above the continuum decreased by $\sim 30\%$ and $\sim 25\%$ for the Sun and Arcturus respectively, as compared with the model excluding collisions with neutral hydrogen. For the second case, however, the emission increased with a similar percentage in the solar model, whereas in Arcturus, the modeled flux maximum doubled its value. Thus, in a star like Arcturus the enhancement effect from highly excited lines (see Sect. 3) dominates the reduction effect from the higher collisional rates in the line transitions themselves, so that when introducing collisions with neutral hydrogen homogeneously throughout the model atom, the outcome is an emission increase (as seen in Fig. 3). We can understand this by noting that, e.g., the ratio between collisional and radiative deexcitation rates for the $8i \rightarrow 7h$ transition (supplying the 12.22 μm line) is $C_{ji}/R_{ji} \sim 15.0$ (Sun) and ~ 0.2 (Arcturus) in typical line-forming layers when collisions with neutral hydrogen are excluded. In principle, this means that the contribution from hydrogen is needed in the giants to ensure an efficient Rydberg ladder.

6.3. Observations of Rydberg emission lines around 12 μm

The observed emission-line flux spectra for Pollux and Arcturus in the 12 μm region closely resembles the solar limb intensity spectrum, whereas the solar disk-center spectrum lacks emission features from other elements than magnesium (see Fig. 5). It is evident that strong emission features from the K giants, as compared with solar-type dwarfs, appear for more metallic Rydberg lines than magnesium, and the observability of different elements so far follows the same pattern as in the Sun. Future observations will tell if this observed trend remains for a larger

sample. Model tests with K dwarfs indeed predict lower Mg I emission for dwarfs than for giants also within the same spectral class (supported as well by observations of the magnetically active K dwarf ϵ Eridani, Richter et al., in preparation).

For cooler K giants, absorption from water vapor starts to influence the 12 μm spectrum and we have detected a blend at 12.32 μm in Arcturus and Aldebaran. Observations from this spectral region in the yet cooler M supergiant Betelgeuse (Ryde et al. 2006) reveal no emission lines above the noise level, which is consistent with our modeling of the Mg I lines in this star (using the same stellar parameters as in Ryde et al.).

6.4. Comparison with other studies

Uitenbroek & Noyes (1996) modeled the Mg I 12.32 μm line in Arcturus and concluded that the computed line was, roughly, half as strong as the observed. When using the 'C92' model, we find an even larger discrepancy for the 12.22 μm line (see Fig. 3). As already discussed, these longstanding discrepancies between observations and models for K giants are removed when using our new model atom. We note also that Uitenbroek & Noyes did not detect the water vapor absorption line, which is blended with the Mg I 12.32 μm line in our Fig. 5. The extension of the model atom changes the results in the solar case as well (as compared with C92 and Ryde et al. 2004), placing the Mg I lines in higher emission, but the former results are recovered by the introduction of collisions with neutral hydrogen.

We have settled here with the rather questioned, albeit standard, Drawin recipe for collisions with neutral hydrogen while we await results from more rigorous quantum mechanical calculations. We have shown the influence from these collisions on the formation of the mid-infrared Mg I emission lines, however we stress that it has not been an aim of this investigation to put detailed empirical constraints on their efficiency. Such a task would require a larger set of lines, including also other wavelength regions. Nevertheless, we may still compare our adopted scaling factor to the Drawin formula for Mg I collisions with neutral hydrogen, $S_{\text{H}} = 10^{-3}$, with other values from the literature. Mentioned in Sect. 4.2 was the exponential decrease resulting in $S_{\text{H}} = 3 \times 10^{-10}$ for the 12 μm transitions (Zhao et al. 1998), a model which was later abandoned by the same group in favor of a constant $S_{\text{H}} = 0.05$ (Gehren et al. 2004), inferred only from optical lines. In a recent non-LTE abundance study of magnesium in metal-poor stars (Mashonkina et al. 2008), $S_{\text{H}} = 0.1$ is used. The value we find based on the mid-infrared lines is more than one order of magnitude lower than the values obtained from these two optical studies. Our model atom has not been applied to optical lines, however such a combined study should be given high priority in future work. We thus conclude that the mid-infrared emission lines from near-by giant stars may be suitable diagnostics for testing atomic input data in future non-LTE analyses.

Finally, as we are now able to model and explain the observed emission lines for both dwarfs and giants, diagnostic applications regarding stellar disk-averaged magnetic fields are possible.

Acknowledgements. We thank M. Carlsson for providing the data and procedures from his model atom, and J. Puls, K. Lind & K. Butler for careful readings and valuable suggestions to the manuscript.

JS gratefully acknowledges a grant from the International Max-Planck Research School of Astrophysics (IMPRS), Garching. NR is Royal Swedish Academy of Sciences Research Fellow supported by a grant from the Knut and Alice Wallenberg Foundation. GH's contribution was supported by NASA ADP grant NNG 04GD33G issued through the Office of Space Science and the NSF US-Sweden Cooperative Research Program grant INT-0318835 to the University

of Colorado. We are also grateful for financial support from The Swedish Foundation for International Cooperation in Research and Higher Education (STINT), grant IG 2004-2074. MR and AK acknowledge the support from the NSF grant AST-0708074.

Observations with TEXES were supported by NSF grant AST-0607312 and we thank the other members of the TEXES team for their assistance. We also acknowledge the excellent support of Gemini and IRTF day and nighttime staff who help make TEXES observations a success. NSO/Kitt Peak FTS data used here were produced by NSF/NOAO.

References

- Allen, C. W. 1973, *Astrophysical quantities* (London: University of London, Athlone Press, —c1973, 3rd ed.)
- Asplund, M. 2005, *ARA&A*, 43, 481
- Avrett, E. H., Chang, E. S., & Loeser, R. 1994, in *IAU Symposium*, Vol. 154, *Infrared Solar Physics*, ed. D. M. Rabin, J. T. Jefferies, & C. Lindsey, 323–+
- Baumüller, D. & Gehren, T. 1996, *A&A*, 307, 961
- Brault, J. & Noyes, R. 1983, *ApJ*, 269, L61
- Bruls, J. H. M. J., Solanki, S. K., Rutten, R. J., & Carlsson, M. 1995, *A&A*, 293, 225
- Carlsson, M. 1986, *Uppsala Astronomical Observatory Reports*, 33
- Carlsson, M. 1992, in *Astronomical Society of the Pacific Conference Series*, Vol. 26, *Cool Stars, Stellar Systems, and the Sun*, ed. M. S. Giampapa & J. A. Bookbinder, 499–+
- Carlsson, M., Rutten, R. J., & Shchukina, N. G. 1992, *A&A*, 253, 567
- Chang, E. S. 1984, *Journal of Physics B Atomic Molecular Physics*, 17, L11
- Chang, E. S. 1994, in *IAU Symposium*, Vol. 154, *Infrared Solar Physics*, ed. D. M. Rabin, J. T. Jefferies, & C. Lindsey, 297–+
- Chang, E. S., Avrett, E. H., Noyes, R. W., Loeser, R., & Mauas, P. J. 1991, *ApJ*, 379, L79
- Chang, E. S. & Noyes, R. W. 1983, *ApJ*, 275, L11
- Cunto, W. & Mendoza, C. 1992, *Revista Mexicana de Astronomía y Astrofísica*, vol. 23, 23, 107
- Decin, L., Vandenbussche, B., Waelkens, C., et al. 2003, *A&A*, 400, 709
- Drake, J. J. & Smith, G. 1991, *MNRAS*, 250, 89
- Drawin, H. W. 1969, *Zeitschrift für Physik*, 225, 483
- Gehren, T., Liang, Y. C., Shi, J. R., Zhang, H. W., & Zhao, G. 2004, *A&A*, 413, 1045
- Gray, D. F. 1976, *The observation and analysis of stellar photospheres* (Research supported by the National Research Council of Canada. New York, Wiley-Interscience, 1976, 484 p.)
- Grevesse, N., Asplund, M., & Sauval, A. J. 2007, *Space Science Reviews*, 130, 105
- Gustafsson, B., Bell, R. A., Eriksson, K., & Nordlund, A. 1975, *A&A*, 42, 407
- Gustafsson, B., Edvardsson, B., Eriksson, K., et al. 2008, *ArXiv e-prints*, 805
- Harper, G. M. 1994, *MNRAS*, 268, 894
- Hoang-Binh, D. & van Regemorter, H. 1994, in *IAU Symposium*, Vol. 154, *Infrared Solar Physics*, ed. D. M. Rabin, J. T. Jefferies, & C. Lindsey, 353–+
- Hoang-Binh, D. & van Regemorter, H. 1995, *Journal of Physics B Atomic Molecular Physics*, 28, 3147
- Lacy, J. H., Richter, M. J., Greathouse, T. K., Jaffe, D. T., & Zhu, Q. 2002, *PASP*, 114, 153
- Lemke, M. & Holweger, H. 1987, *A&A*, 173, 375
- Mashonkina, L., Zhao, G., Gehren, T., et al. 2008, *A&A*, 478, 529
- Mashonkina, L. J. 1996, in *Astronomical Society of the Pacific Conference Series*, Vol. 108, *M.A.S.S., Model Atmospheres and Spectrum Synthesis*, ed. S. J. Adelman, F. Kupka, & W. W. Weiss, 140–+
- Mauas, P. J., Avrett, E. H., & Loeser, R. 1988, *ApJ*, 330, 1008
- Moccia, R. & Spizzo, P. 1988, *Journal of Physics B Atomic Molecular Physics*, 21, 1133
- Omont, A. 1977, in *Physics of Electronic and Atomic Collisions: ICPEAC X*, 166–+
- Pengelly, R. M. & Seaton, M. J. 1964, *MNRAS*, 127, 165
- Przybilla, N., Butler, K., Becker, S. R., & Kudritzki, R. P. 2001, *A&A*, 369, 1009
- Rutten, R. J. & Carlsson, M. 1994, in *IAU Symposium*, Vol. 154, *Infrared Solar Physics*, ed. D. M. Rabin, J. T. Jefferies, & C. Lindsey, 309–+
- Ryde, N., Harper, G. M., Richter, M. J., Greathouse, T. K., & Lacy, J. H. 2006, *ApJ*, 637, 1040
- Ryde, N., Korn, A. J., Richter, M. J., & Ryde, F. 2004, *ApJ*, 617, 551
- Ryde, N., Lambert, D. L., Richter, M. J., & Lacy, J. H. 2002, *ApJ*, 580, 447
- Seaton, M. J. 1962, in *Atomic and Molecular Processes*, ed. D. R. Bates, 375–+
- Sigut, T. A. A. & Lester, J. B. 1996, *ApJ*, 461, 972
- Smith, M. A. & Dominy, J. F. 1979, *ApJ*, 231, 477
- Steenbock, W. & Holweger, H. 1984, *A&A*, 130, 319
- Uitenbroek, H. & Noyes, R. W. 1996, in *Astronomical Society of the Pacific Conference Series*, Vol. 109, *Cool Stars, Stellar Systems, and the Sun*, ed.

- R. Pallavicini & A. K. Dupree, 723–+
van Regemorter, H. 1962, ApJ, 136, 906
Zhao, G., Butler, K., & Gehren, T. 1998, A&A, 333, 219